Electronic Supplementary Material (ESI) for Physical Chemistry Chemical Physics.
This journal is © the Owner Societies 2016

Specific Cation Interactions as the Cause of Slow Dynamics and Hysteresis in Dye and Perovskite Solar Cells: a Small-Perturbation Study

Lidia Contreras [a], *Jesús Idígoras* [a,*], *Anna Todinova* [a], *Manuel Salado* [b], *Samrana Kazim* [b],
Shahzada Ahmad [b], *Juan A. Anta* [a,*]

[a] Área de Química Física, Universidad Pablo de Olavide, Sevilla, Spain.

[b] Abengoa Research, C/Energía Solar n° 1, Campus Palmas Altas, 41014 Sevilla, Spain

Table S1. Composition of the electrolytes for the DSSCs studied in this work.

Electrolyte	**Solvent (v/v, %)**	**Solutes**
Acn	100% Acetonitrile	0.03M I_2 + 1M BMII + 0.05M LiI + 0.5M TBP + 0.1M GuSCN
Pyr50	50% Acn + 50% RTIL	
Pyr75	25% Acn + 75% RTIL	
Pyr100	100% RTIL	

I_2: Iodine,BMiI:1-butyl-3-methylimidalozliumiodide,LiI: Lithium iodide, TBP: 4-tert-butylpiridine, GuSCN: Guanidine thiocyanate, Acn: Acetonitrile, Pyr: 1-Buthyl-1-Methylpyrrolidinium bis(trifluoromethanesulfonyl)imide.

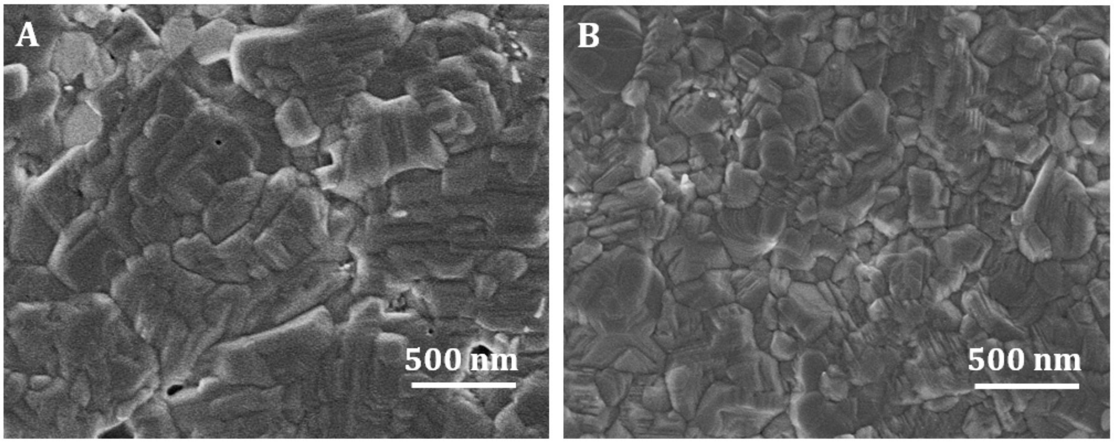

Figure S1: Plane-view scanning electron microscopy (SEM) images for the (A) $MAPbI_3$ and (B) $MA_{0.6}FA_{0.4}PbI_3$ perovskite layers.

Table S2. Photovoltaic parameters measured under 1 sun - AM 1.5 illumination for the different devices. Error bars are estimated from the results of three devices of the same configuration.

	Jsc (mA·cm^{-2})	**Voc (mV)**	**Fill Factor**	**Efficiency (%)**
Acn	13.4 ± 0.2	770± 8	68± 2	7.0 ± 0.2
Pyr50	12.3 ± 0.2	721 ±9	59± 1	5.2 ± 0.1
Pyr75	2.8 ± 0.4	680±12	72 ± 2	1.5± 0.1
Pyr100	1.5± 0.2	675± 5	66± 3	0.6 ± 0.2
MAI	20 ± 0.7	980 ± 20	70 ± 4	13.5 ± 1
MAI/FAI	19.9 ± 0.4	885 ± 30	66 ± 1	11.5 ± 0.5

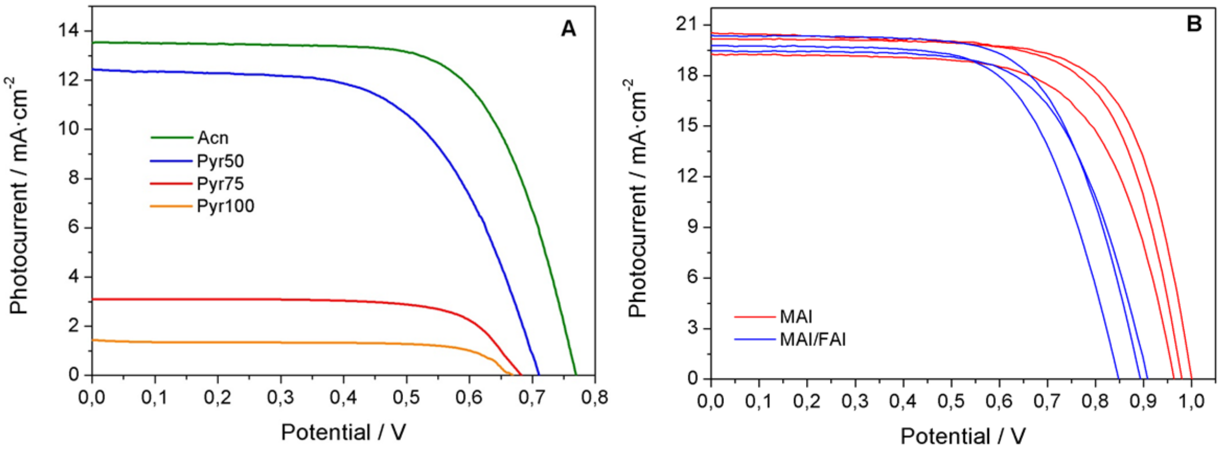

Figure S2. Current-voltage curves of the different (A) DSSCs and (B) PSCs under 1 sun - AM 1.5 illumination in forward scan and reverse scan, respectively. Scan rate of 35mV/s and 100mV/s with a waiting time of 30s at 1V and 1.2V were employed for DSSCs and PSC, respectively.

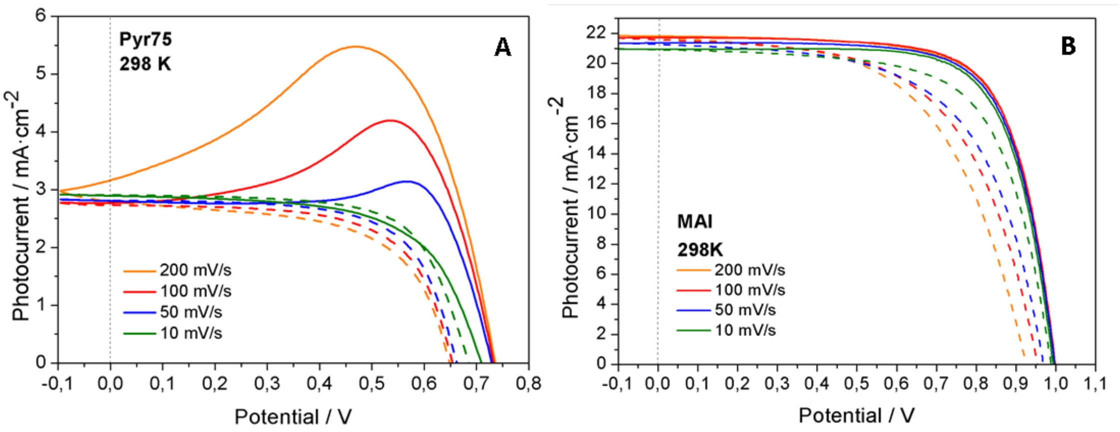

Figure S3. Current-voltage curves of Pyr75 and MAI devices measured in the reverse scan (line) and forward scan (dash line) under light intensity of 10 mW·cm^{-2} using a green LED.

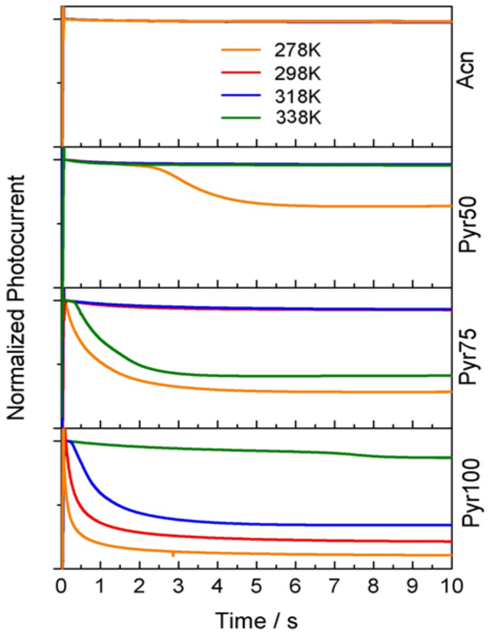

Figure S4. Time-dependence photocurrent density for different DSSCs at different temperatures measured under light intensity of 10 mW·cm^{-2} using a green LED.

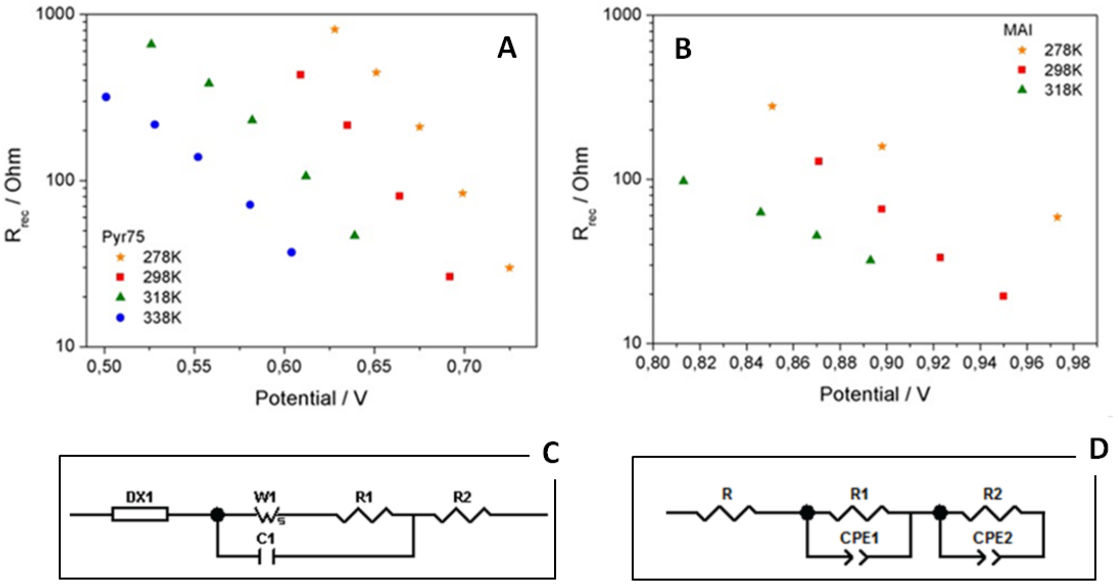

Figure S5. Electron recombination resistance data as extracted from impedance spectroscopy measurements for (A) Pyr75 and (B) MAI samples. Equivalent circuits used for the fitting of the impedance spectra for (C) DSSCs (transmission line model, where DX1 is the distributed element for the diffusion-recombination transmission line [see J. Bisquert, J. Phys. Chem. B, 2002, 106, 325] R1 is charge transfer resistance, C1 is double layer capacitance, W1 is Warburg diffusion impedance and R2 is series resistance) and (D) PSCs (R-CPE model, where R is series resistance, and CPE is constant phase elements.

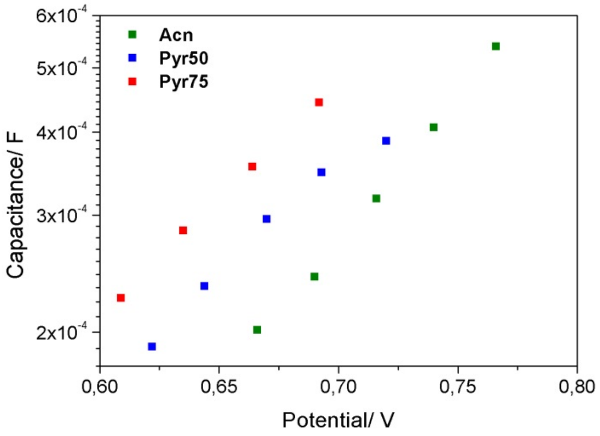

Figure S6. Chemical capacitance data as extracted from impedance spectroscopy measurements for DSSCs using the transmission line model.

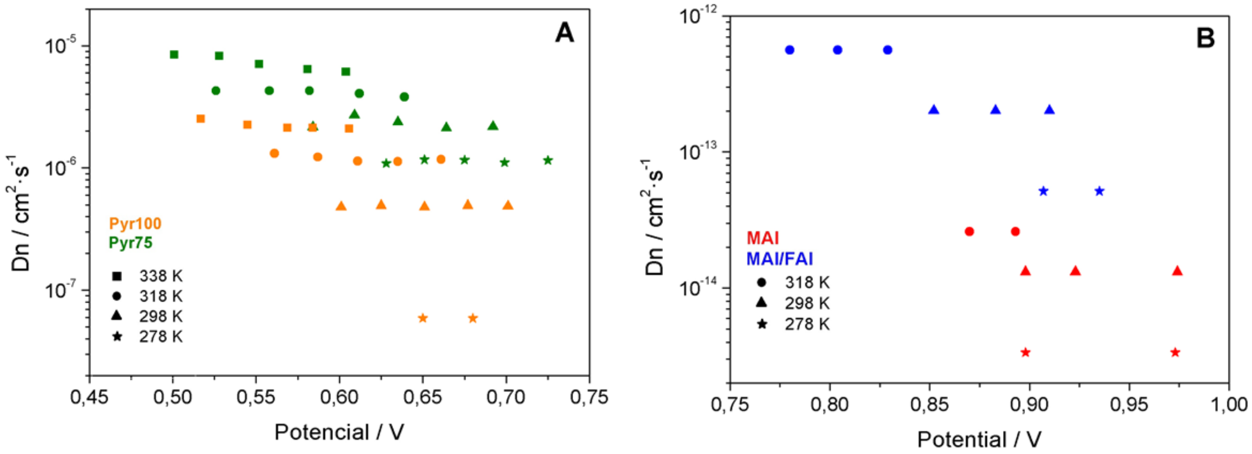

Figure S7. Ionic diffusion coefficients data as extracted from impedance spectroscopy measurements for (A) DSSCs and (B) PSCs.

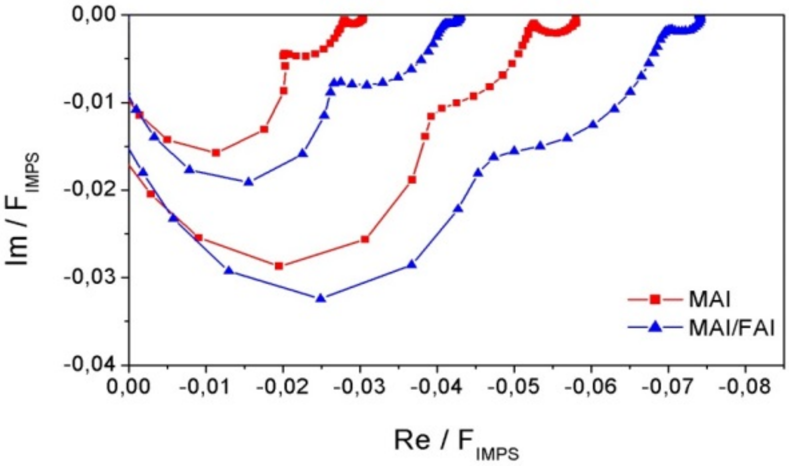

Figure S8. IMPS response of the both perovskites at two different illumination intensities.

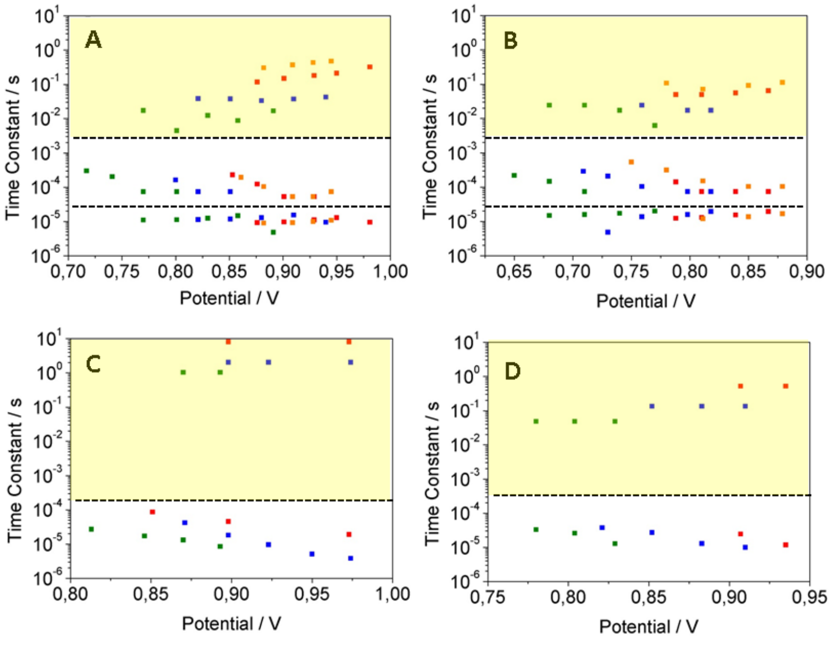

Figure S9. Characteristic time constants extracted from (A, B) IMPS and IS (C, D) frequency plots for (A,C) MAI and (B, D) MAI/FAI samples at different temperatures: (green) 318K, (blue) 298K, (red) 278K and (orange) 258K.

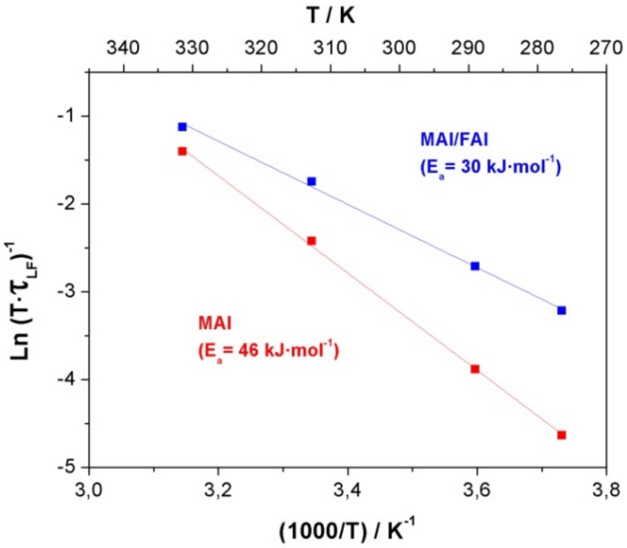

Figure S10. Arrhenius-like plot $\ln(T/\tau_{LF})^{-1}$ versus 1000/T for MAI and MAI/FAI devices. τ_{LF} was extracted from IMPS low-frequency component.

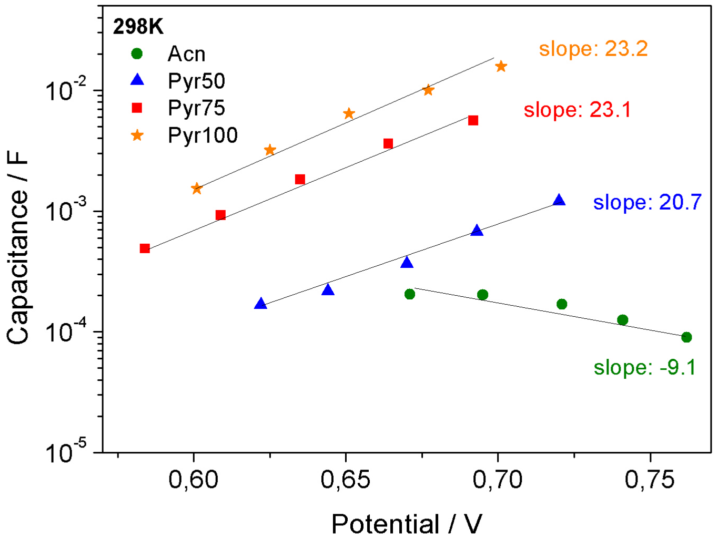

Figure S11. Low-frequency capacitance (Figure 3C) with respect to open-circuit potential extracted for the different DSSC compositions studied. The labels indicate the slope in V^{-1} extracted from both data sets.